iScience

CellPress
OPEN ACCESS

Article

Stacks of monogalactolipid bilayers can transform into a lattice of water channels

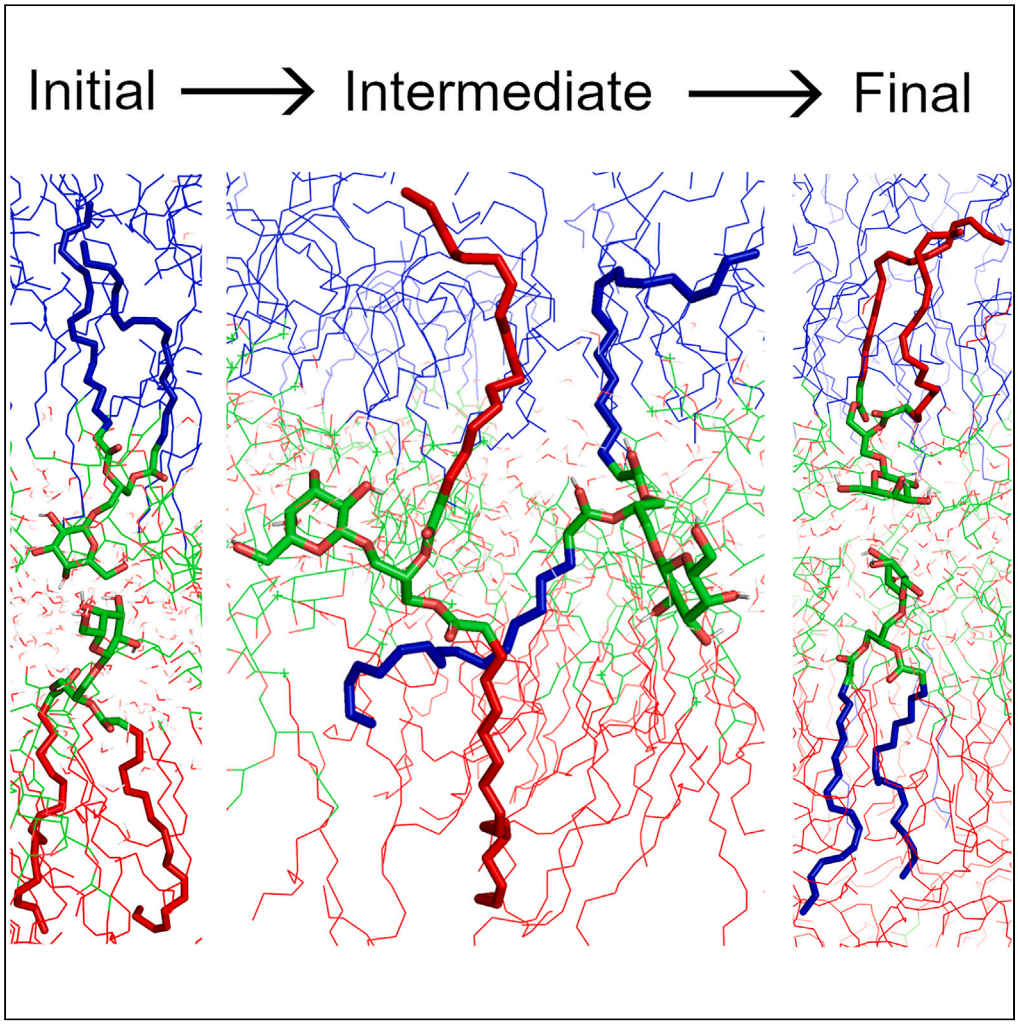

Jakub Hryc, Michal Markiewicz, Marta Pasenkiewicz-Gierula

jakub.hryc@doctoral.uj.edu.pl (J.H.)
marta.pasenkiewicz-gierula@uj.edu.pl (M.P.-G.)

Highlights

Nine stacks of MGDG bilayers with varying inter-bilayer water content are MD simulated

Lamellar/nonlamellar phase transition depends on the widths of adjacent water layers

Water channels form due to bilayer bending and inter-bilayer MGDG-MGDG interactions

MGDG molecules swap locally between apposing leaflets in a concerted manner

Hryc et al., iScience *26*, 107863
October 20, 2023
https://doi.org/10.1016/j.isci.2023.107863

iScience

CellPress
OPEN ACCESS

Article

Stacks of monogalactolipid bilayers can transform into a lattice of water channels

Jakub Hryc,[1,3,*] Michal Markiewicz,[1] and Marta Pasenkiewicz-Gierula[1,2,*]

SUMMARY

The lipid matrix of thylakoid membranes is a lamellar bilayer, but under a certain condition it can convert locally into a nonlamellar structure. This is possible because one of the main membrane lipids, MGDG, promotes the formation of an inverse hexagonal phase. Here, the spontaneous transformation of aligned hydrated MGDG bilayers into nonlamellar structures is investigated using all-atom molecular dynamics simulation. Previous studies have demonstrated that MGDG polar head groups connect vertically across the interface. In this study, the evolution of the system's initial structure into a lattice of water channels and contacted surfaces created by numerous vertical MGDG connections depended on the width of the hydrating water layers. These widths controlled the bilayers' ability to bend, which was a prerequisite for channel formation. Locally, an intensive exchange of MGDG molecules between apposing bilayer leaflets occurred, although a stable semi-toroidal stalk did not develop.

INTRODUCTION

The lipid matrix of plant thylakoid membranes is composed of two neutral galactolipids, monogalactosyldiacylglycerol (MGDG, ~50%) and digalactosyldiacylglycerol (DGDG, ~20%–30%), as well as two less represented (~20%–40%), anionic lipids, namely sulfoquinovosyldiacylglycerol (sulfolipid, SQDG) and phosphatidylglycerol (PG).[1,2] The matrix is a lamellar structure, even though the two main lipids, MGDG and DGDG, have opposite phase tendencies. These tendencies follow from their chemical structures. The head group of MGDG contains β-D-galactose and that of DGDG additionally contains α-D-galactose. Their acyl chains are commonly 18-carbon triple-*cis*-unsaturated (18:3-*cis*).[3] In effect, di-18:3-*cis* DGDG has a cylindrical shape and a tendency to form a lamellar bilayer in water,[4] whereas di-18:3-*cis* MGDG (Figure 1) has a cone shape and a tendency to form an inverse hexagonal phase (H_{II}).[5,6]

The H_{II} phase forms in the process of spontaneous aggregation of nonbilayer lipids, such as MGDG or phosphatidylethanolamine (PE) when dispersed alone or in a mixture with other lipids, in water.[7] This phase consists of an ordered lattice of hexagonally packed water cylinders surrounded by lipid molecules. Their heads face the water and form the wall of each cylinder, whereas the hydrocarbon chains spread outward and fill the inter-cylinder space.[5,7,8]

The H_{II} phase can also emerge as a result of L_α/H_{II} phase transition of aligned lamellar bilayers (L_α).[9–11] As the L_α/H_{II} transition and membrane fusion[12,13] proceed similarly, it has rationally been assumed that they pass through the same intermediate state[13–16] called a stalk.[17] A stalk is a locally formed semi-toroidal lipid connection between apposing leaflets of two bilayers.[18,19] In bilayers containing the non-bilayer lipids PE[9] and MGDG[20] stalks form spontaneously. In other lipid bilayers, they can form only when the bilayer surfaces are sufficiently dehydrated;[21] this is because the inter-bilayer water prevents close contact between neighboring bilayers. Moreover, water molecules that bind to the lipid polar groups effectively compete with lipid-lipid interactions. To enable inter-bilayer lipid-lipid connections that are necessary for stalk formation, the inter-bilayer water has to be removed. Natural membranes fuse with the help of fusogenic v-SNARE and t-SNAREs proteins[22–24] that bring them together and dehydrate. Bilayers containing negatively charged cardiolipin or phosphatidic acid can transform into a nonlamellar phase in the presence of divalent ions.[8,25]

An alternative mechanism of membrane fusion and L_α/H_{II} phase transition is based on an extended (splayed-chain) lipid conformation that was first proposed by Kinnunen[14] and later elaborated in Refs.[11,26]. The involvement of the splayed-chain lipid conformation in initiating bilayer fusion has been demonstrated in computer simulations[27,28] and experimentally[29,30] but the fusion itself did not proceed as proposed in.[14]

[1]Department of Computational Biophysics and Bioinformatics, Faculty of Biochemistry, Biophysics and Biotechnology, Jagiellonian University, 30-387 Krakow, Poland
[2]Senior author
[3]Lead contact
*Correspondence: jakub.hryc@doctoral.uj.edu.pl (J.H.), marta.pasenkiewicz-gierula@uj.edu.pl (M.P.-G.)
https://doi.org/10.1016/j.isci.2023.107863

In this study, the formation of water channels induced by strong vertical links between MGDG molecules from apposing leaflets in the system initially consisting of aligned MGDG bilayers is investigated using all-atom molecular dynamics (MD) simulation. These channels should be thought of as locally connected poorly hydrated and locally bent fully hydrated fragments of the neighboring bilayers in the form of water-filled tubes. This nonlamellar phase is possibly a transient state in L_α/H_{II} phase transition and consists only of lipid and water molecules. These lipid-based water channels accumulate rather than transport water, unlike aquaporins, intrinsic membrane proteins, also called water channels, whose main biological function is the controlled transport of water across cell membranes.[31] They should also be distinguished from water nanochannels that can be used as selective fillers in specially designed desalination and water treatment membranes.[32]

The choice of subject was motivated by the role of MGDG in biophysical processes that take place in thylakoid membranes. MGDG, due to its shape, high negative intrinsic curvature, and high propensity to form lipid-lipid hydrogen bonds, promotes stacking of thylakoids into grana by forming intermembrane stalks,[20] induces a curvature stress in thylakoid membranes,[33,34] affects their curvature,[35] and plays a major role in their structural dynamics,[36] although the extreme curvature of the grana margins is induced mainly by CURT1 proteins.[37] Moreover, there is *in vitro* experimental evidence that the H_{II} phase plays a crucial role in the xanthophyll cycle, e.g.,[38–40] MGDG, as a main lipid component of thylakoid membranes and a H_{II} phase promoting lipid, is very likely involved in this process.

MD simulation studies on galactolipid polymorphism carried out so far have used a coarse-grained lipid model, e.g., Refs.[41–44]. In contrast, an all-atom galactolipid model is consistently applied in our studies of both lamellar[45–48] and nonlamellar[49,50] phases.

The goal of this study is to investigate, on the molecular and atomic level, when and how the initial lamellar system consisting of aligned MGDG bilayers evolved into a structure consisting of water-filled channels that extend horizontally across the system and form a hexagonal-like lattice. Elucidation of this process could help in better understanding how the formation of nonlamellar lipid structures in general and in thylakoid membranes in particular proceeds. In the thylakoids, these structures are called the H_{II} phase, but they should rather be recognized as locally formed water-filled cylinders necessary for the xanthophyll cycle to occur, e.g., Refs.[38,40]. Their presence has been indirectly evidenced experimentally,[36,38] although how they form and what their precise architecture is remains rather obscure. More generally, nonlamellar lipid phases are common in biomembranes and play important roles in cellular processes.[51–53] They are also used as carriers in drug delivery,[54] thus the atomic-level details of the nonbilayer phase formation revealed in this study should deepen understanding of the important purely biotechnological processes that involve nonlamellar lipid phases.

This study provides evidence that the necessary condition for the channels to form is strong vertical connections between MGDG molecules from apposing leaflets and bending of the bilayers. The bending depends on the widths of the water layers in a multibilayer system simulated under periodic boundary conditions (PBC). However, it does not show that on a microsecond timescale semitoroidal lipid stalks form between apposing leaflets, even though MGDG molecules exchange locally between leaflets via extended lipid conformations. The lipid exchange between lipid bilayers is an indispensable step in membrane fusion, a fundamental biological process that takes place in each living cell and is also utilized in drug delivery.

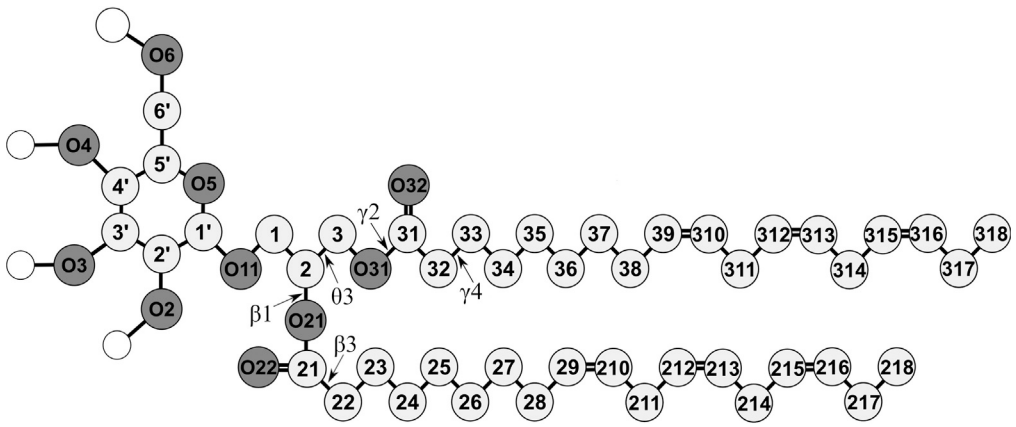

Figure 1. Molecular structures of di-18:3-*cis* MGDG

The acyl chains and glycerol atoms are numbered according to Sundaralingam's nomenclature[55] (the positions of atoms C1 and C3 are swapped relative to the *sn* convention). The galactose atoms are numbered according to the IUPAC convention.[56] The galactose carbon atoms are marked with ′ to distinguish them from the C1, C2, and C3 atoms of the glycerol. The chemical symbol for carbon atoms, C, is omitted, and the hydrogen atoms are not shown except for the polar ones shown as empty circles. Oxygen (O) atoms are dark, and the carbon atoms are light gray circles, respectively. Some of the torsion angles discussed in the text are marked, θ3 in the glycerol backbone, β1 and β3 in the β (*sn*-2) chain, and γ2 and γ4 in the γ (*sn*-1) chain.

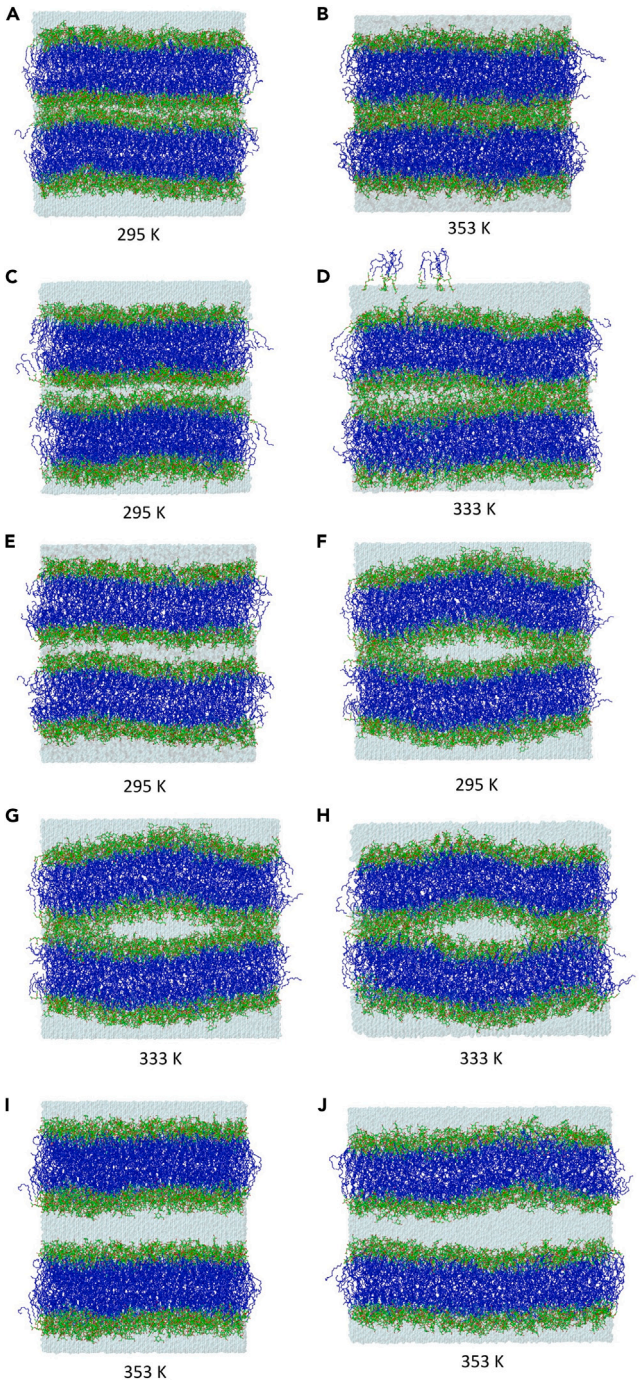

Figure 2. Snapshots of double bilayers with different numbers of water molecules in the inner and the outer water layer

(A–J) Initial (A, C, E, G, I) and final, after 585, 700, 320, 820, and 500 ns of simulation (B, D, F, H, J, respectively) structures of double bilayers. W8-30 (A, B), W12-30 (C, D), W15-30 (295 K, E, F), W15-30 (333 K, G, H), and W30-30 (I, J) (see text). The atoms are represented in standard colors, except for the acyl chain carbon atoms, which are dark *blue*. The water is shown as a transparent *blue* surface. The MGDG hydrogen atoms are not shown. The temperature corresponding to each structure is given below the structure.

Models

The initial structure of the MGDG bilayer was constructed using the Packmol program[57] from scratch in.[50] The bilayer consisted of 450 MGDG molecules (2 × 15×15) and 13,500 water molecules (30 H_2O/MGDG). The all-atom models of the MGDG molecule and the MGDG bilayer

were validated previously.[45,50] When creating simulation systems for this study, the last frame of the MGDG bilayer simulated in Ref.[50] (single bilayer) was used.

Double bilayer

The double bilayer consisting of two MGDG bilayers was constructed by duplicating the single MGDG bilayer, placing one bilayer above the top of the other and rehydrating them with a chosen number of water molecules.

Outer layer with fixed, inner layer with varied numbers of H_2O/MGDG. Four such double bilayers were constructed (Figures 2A–2J). In all systems, the outer water layer (outside the bilayers but common via PBC, cf. STAR Methods) contained 13,500 H_2O molecules (30 H_2O/MGDG). The intra-bilayer water layer (inner layer) contained 3,600 (8 H_2O/MGDG, W8-30); 5,400 (12 H_2O/MGDG, W12-30); 6,750 (15 H_2O/MGDG, W15-30); or 13,500 (30 H_2O/MGDG, W30-30) water molecules.

The same number of H_2O/MGDG in outer and inner layers. Three such double bilayers were constructed (Figures 3A–3F). In these systems, the inner and the outer water layer contained 3,600 (8 H_2O/MGDG, W8-8); 5,400 (12 H_2O/MGDG, W12-12); or 6,750 (15 H_2O/MGDG, W15-15) water molecules.

Quadruple bilayer

The quadruple bilayer (Figures 4A–4D) consisting of four MGDG bilayers was constructed by duplicating the last frame of the W15-15 double bilayer simulated for 500 ns and placing one on top of the other. Each water layer contained 6 750 H_2O (15 H_2O/MGDG, 2xW15-15).

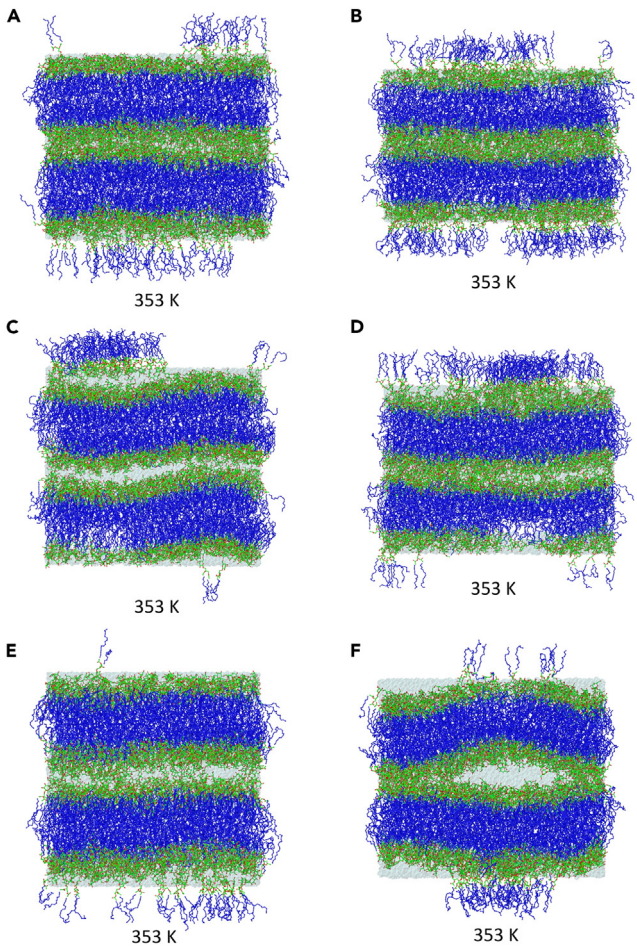

Figure 3. Snapshots of double bilayers with the same number of water molecules in the inner and the outer water layer

(A–F) Initial (A, C, E) and final, after 1000, 500, 1000 ns of simulation (B, D, F, respectively) structures of double bilayers. W8-8 (A, B), W12-12 (C, D), W15-15 (E, F). Other details as in Figure 2.

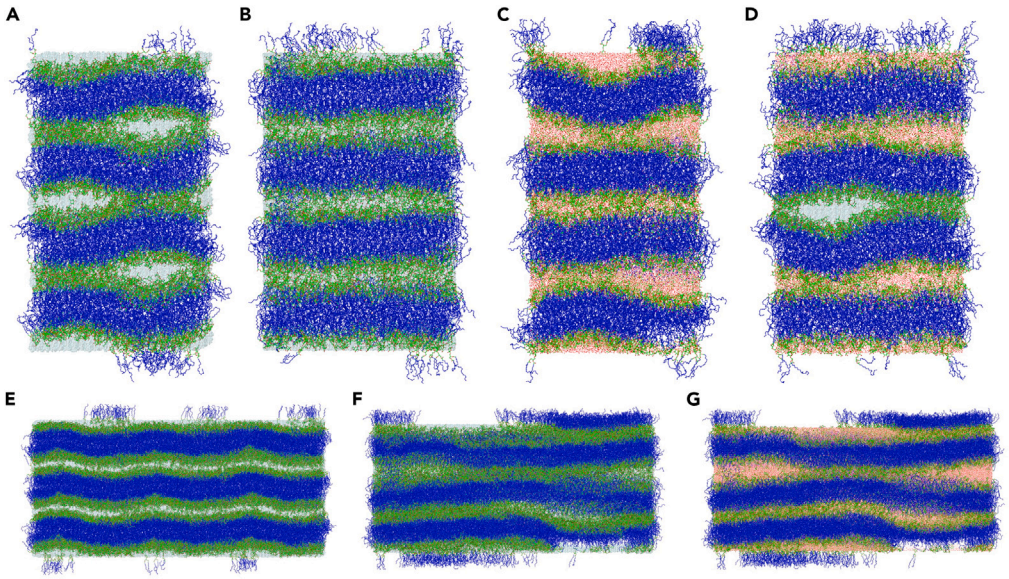

Figure 4. Snapshots of quadruple and triple bilayers

(A–G) Initial (A, B, E) and final, after 1000 ns of simulation (C, D, F, G) structures of 2xW15-15 (A, B, C, D) and 6xW15-15-15 (E, F, G) systems. To show the direction of the water channels in 2xW15-15, (A, C) are the front (*x*,*z*-plane) and (B, D) are the side (*y*,*z*-plane) views. (E, F, G) are the front views of 6xW15-15-15. In (A, B, E, F, and partially in D) the water is shown as a transparent *blue* surface; to show the water-filled channels better, in (C, G, and partially in D) the water molecules are shown explicitly to expose the water-filled caves better. Other details as in Figure 2.

Triple bilayer

To build the triple bilayer (Figures 4E–4G), five copies of the single bilayer were created; two of them were placed adjacent to the bilayer along the x axis and the other three behind them, in the *x*-*y* plane (45 × 30 MGDG in each leaflet). Then, two copies of the enlarged system, one after the other, were placed on top of it. Each water layer contained 40,500 H_2O molecules (15 H_2O/MGDG, 6xW15-15-15).

The numbers of lipid and water molecules in the models and the width of each water layer together with some simulation conditions/parameters are summarized in Table S1; the main details are also given in Tables 1 and 2. The width of each water layer was estimated as the distance between the cross-points of the lipid and water density distributions in the double bilayer, as is shown in Figure S1A and described in STAR Methods.

RESULTS

There are two major aims of the analyses of the systems of aligned MGDG bilayers described earlier. One is to determine the level of hydration of the bilayers necessary for water channels to form spontaneously. The other is to reveal the molecular level details of the exchange of MGDG molecules across a polar interfacial region. The formation of water channels requires multiple, strong, and locally extended vertical connections between the MGDG molecules from apposing leaflets. A comprehensive analysis in Ref.[50] reveals, that MGDG molecules connect across the interface by forming direct hydrogen (H-) bonds, or water bridges, or both between their head groups (Figure S2). In the analyses below, only pairs of vertically connected MGDG molecules are considered, irrespective of how many individual short-range interactions (H-bonds and water bridges) link two molecules in the pair. These inter-lipid connections are very dynamic—they form and break constantly. Nevertheless, the number of vertically connected pairs of MGDG molecules (vertical MGDG pairs), after initial growth, is stable (Figures 5 and S3–S7).

In this simulation study, water channels are horizontally oriented water-filled tubes that form between two adjacent bilayers and cross the whole system along one of the system's horizontal axes (*x* or *y*). The tubes are separated by connected surfaces created by numerous vertical MGDG pairs, and their cross-sections are more lenticular than circular, cf. Figures 2, 3, and 4. The formation of a water-filled channel is coupled with the bending of the bilayers.

Water channel formation and level of hydration

Double bilayer, outer layer with fixed, inner layer with varied numbers of H_2O/MGDG

The W8-30 double bilayer containing 8 H_2O/MGDG in the inner, 3.4 Å wide, and 30 H_2O/MGDG in the outer, 23.6 Å wide, water layer (Figures 2A and 2B) was simulated at 295 K (30 ns), then at 333 K (52.5 ns) with anisotropic pressure control (aniso), and finally at 353 K (500 ns) with semiisotropic pressure control (Table 1); 353 K (80°C) is the highest temperature at which an experimental study on MGDG polymorphism has been carried out.[5] The motivation for using higher temperatures and different simulation protocols at different temperatures is given in STAR Methods.

Vertical MGDG pairs across the inner water layer formed almost immediately at the start of the simulation at 295 K (Figure 5A). Their number increased to a stable value of ~310 in less than 30 ns (Figure 5A; Table 3) and did not change significantly at higher temperatures (Figures 5B and 5C; Table 3). The close contact between the vertically paired head groups was confirmed by a significant overlap of their density profiles along the W8-30 normal (Figure S1B). In contrast, no vertical pairs formed across the outer water layer during the simulation; consequently, the density profiles of the rings of MGDG from the outer leaflets remained separated (Figure S1B).

The vertical MGDG pairs involved virtually all MGDG molecules in each of the inner leaflets, i.e., 225. The number of MGDG molecules in a leaflet was smaller than the number of vertical pairs (~310) because one MGDG molecule from a leaflet could connect to more than one in the opposite leaflet (Figure S2). At each temperature, the numerous and strong inter-lipid vertical interactions created one firm connected surface that prevented the bilayers from bending, hence the formation of water channels was inhibited. Moreover, a comparison of the number of water molecules in the inner water layer (8 H_2O/MGDG) with that which each MGDG molecule in the bilayer binds on average (7.14 ± 0.09 H_2O/MGDG[50]) implies that almost all water molecules from the inner layer were bonded to the lipids; in effect, there were no "free" water molecules to form a channel.

Table 1. Simulation systems and parameters for the double bilayers with a fixed number of H_2O/MGDG in the outer water layer

System name	#H_2O/lipid (width [Å]) Inner	#H_2O/lipid (width [Å]) Outer	Temperature [K]/pressure control/simulation time [ns]
W8-30	8 (3.4)	30 (23.6)	295/aniso/30 333/aniso/52.5 353/semi/500
W12-30	12 (8.4)	30 (23.6)	295/aniso/200 333/aniso/500
W15-30	15 (11.3)	30 (23.6)	295/aniso/320 333/semi/500
W30-30	30 (23.6)	30 (23.6)	353/aniso/500

The numbers of water molecules per lipid (#H_2O/lipid) in the inner (Inner) and the outer (Outer) water layer, additionally, estimated widths (width) of each water layer are given in parentheses. Temperature, pressure control algorithm (anisotropic [aniso] or semiisotropic [semi]), and time length of each simulation are given in the 4th column. See also Table S1.

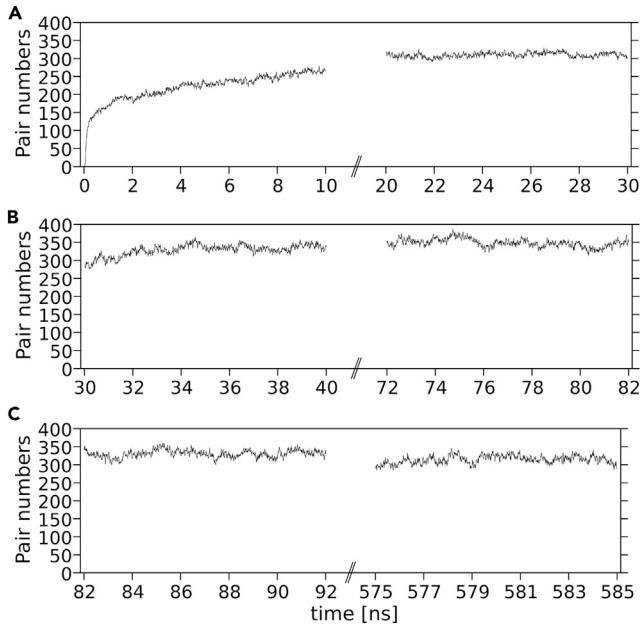

Figure 5. Time profiles of the number of vertical MGDG pairs linking the inner leaflets of W8-30

(A–C) (A) 295 K (30-ns simulation, aniso); (B) 333 K (52.5-ns simulation, aniso); (C) 353 K (500-ns simulation, semi). At each temperature, the pairs were counted during the first and the last 10-ns period of simulation every 1 ps; each point on the plot is a 10-ps average. Each bilayer leaflet contained 225 MGDG molecules. See also Figures S3–S7 and Table 3.

The W12-30 double bilayer containing 12 H_2O/MGDG in the inner, 8.4 Å wide, and 30 H_2O/MGDG in the outer, 23.6 Å wide, water layer (Figures 2C and 2D) was simulated at 295 K for 200 ns and then at 333 K for 500 ns, using anisotropic pressure control (Table 1). In W12-30, as in W8-30, vertical MGDG pairs formed almost immediately and only across the inner water layer, but in a much smaller number (Figure S3). At both temperatures, their average saturating numbers were ~170 (Figures S3A and S3B; Table 3). The fewer vertical MGDG pairs in W12-30 than in W8-30 were additionally illustrated by a smaller overlap of the head group density profiles (Figure S1D).

The 50% smaller number of connected pairs in W12-30 than in W8-30 implies that in W12-30 only half of the MGDG molecules in the inner leaflets were connected. These connections, due to their dynamics, formed a "floating" rather than a firm connected surface, although it prevented the bilayers from sufficient bending. Thus, instability of the vertical MGDG pairs and too small a number of water molecules able to form a channel were the reasons why a stable water channel did not emerge.

The W15-30 double bilayer containing 15 H_2O/MGDG in the inner, 11.3 Å wide, and 30 H_2O/MGDG in the outer, 23.6 Å wide, water layer was simulated at 295 K (320 ns) using anisotropic pressure control (Figures 2E and 2F), then at 333 K (500 ns) using semiisotropic pressure control (Figures 2G and 2H) (cf. STAR Methods). In W15-30, as in the previous systems, vertical MGDG pairs formed across the inner water layer only. Their number grew slowly to a steady value (Figures S4A and S4B; Table 3), and with its increase, a stable water channel emerged within ~50 ns (Figures 2F–2H). This was possible because the outer water layer was wide enough to enable the bilayers to bend, and the inner layer contained enough unbound water molecules to form the channel. Roughly estimated numbers of water molecules and MGDG head groups in the channel were 5230 $\pm$ 90 and 278 $\pm$ 3, respectively, which gave 18.8 $\pm$ 0.3 H_2O/MGDG in the channel and 8.8 $\pm$ 0.5 H_2O/MGDG in the remaining locally flat, partially dehydrated fragments of the inner leaflets. The latter number indicates that the flat fragments created, as in W8-30, firm connected surfaces, which stabilized the channel at both temperatures (Figures 2F and 2H).

The W30-30 double bilayer containing 30 H_2O/MGDG both in the inner and the outer, 23.6 Å wide, water layer (Figures 2I and 2J) was simulated at 353 K for 500 ns. In line with the results above, during the simulation time neither vertical MGDG pairs nor water channels formed.

Double bilayer, the same number of H_2O/MGDG in outer and inner layers

The W8-8 double bilayer containing 8 H_2O/MGDG both in the inner and the outer, 3.4 Å wide, water layer (Figures 3A and 3B) was simulated at 353 K for 1000 ns (Table 2). In W8-8, as in W8-30, vertical MGDG pairs appeared almost immediately, but in contrast, they formed across both the inner and the outer water layer. Their respective numbers of ~318 and ~340 (Figure S5) were similar to that of ~314 in W8-30 (Table 3). Also, the overlap of the density profiles of the MGDG rings along the normal in W8-8 and W8-30 was similar (Figures S1C and S1B). Thus, the reasons why water channels did not form in W8-8 were the same as in W8-30.

Table 2. Simulation systems and parameters for the multibilayers with the same number of H_2O/MGDG in the inner and outer water layers

System name	# Bilayer	#H_2O/lipid (width [Å]) Inner	#H_2O/lipid (width [Å]) Outer	Temperature [K]/pressure control/ simulation time [ns]
W8-8	2	8 (3.4)	8 (3.4)	353/semi/1000
W12-12	2	12 (8.4)	12 (8.4)	353/semi/500
W15-15	2	15 (11.3)	15 (11.3)	353/semi/1000
2xW15-15	4	15 (11.3)	15 (11.3)	353/semi/1000
6xW15-15-15	3	15 (11.3)	15 (11.3)	353/aniso/1000

The numbers of bilayers (# Bilayer) in the system; water molecules per lipid (#H_2O/lipid) in each inner (Inner) and the outer (Outer) water layers, additionally, estimated widths (width) of each water layer are given in parentheses. Temperature, pressure control algorithm (anisotropic [aniso] or semiisotropic [semi]), and time length of each simulation are given in the 5th column. See also Table S1.

The W12-12 double bilayer containing 12 H_2O/MGDG both in the inner and the outer, 8.4 Å wide, water layer (Figures 3C and 3D) was simulated at 353 K for 500 ns (Table 2). In W12-12, as in W8-8, vertical MGDG pairs formed across both the inner and the outer water layer. The average numbers of pairs across each layer in W12-12 and their dynamics, and the overlapping of the head groups density profiles, were essentially the same as those across the inner water layer in W12-30 (Figures S1E, S1D, S3, and S6; Table 3). Thus, the reasons why water channels did not form in W12-12 were the same as in W12-30.

The W15-15 double bilayer containing 15 H_2O/MGDG both in the inner and the outer, 11.3 Å wide, water layer (Figures 3E and 3F) was simulated at 353 K for 1 μs (Table 2). The process of vertical MGDG pairs and water channel formation and its time course in W15-15 were similar to those in W15-30, but in W15-15 it took place in both the inner and outer water layers (Figure S7). In effect, two stable, diagonally shifted, water channels emerged, each in one interface (Figure 3F). The channels were horizontally sealed by firm connected surfaces, which is more visible in Figure 4A, where W15-15 is vertically conjoined with its replica.

During the course of simulation some of the MGDG molecules from the outer leaflets swapped (exchanged) between the leaflets (Figure 6A; film Video S1). The vigorous exchange started at ~350 ns and somehow died away at 900 ns of simulation and involved splaying of the acyl chains (Figures 6 and S9).

Table 3. Equilibrium numbers of vertical MGDG pairs

System	295 K inner/outer (av. period)	333 K inner/outer (av. period)	353 K inner/outer (av. period)
W8-30	309.7 ± 6.8/0 (20–30 ns)	348.6 ± 11.5/0 (42.5–52.5 ns)	314.3 ± 11.5/0 (575–585 ns)
W12-30	167.8 ± 8.3/0 (190–200 ns)	175.0 ± 7.9/0 (490–500 ns)	—
W15-30	111.4 ± 6.0/0 (310–320 ns)	139.4 ± 12.9/0 (810–820 ns)	—
W30-30	—	—	0/0
W8-8	—	—	317.9 ± 10.7/342.5 ± 12.6 (990–1000 ns)
W12-12	—	—	177.4 ± 13.2/158.8 ± 9.7 (490–500 ns)
W15-15	—	—	130.54 ± 7.20/176.1 ± 10.2 (990–1000 ns)

Equilibrium time average numbers of vertical MGDG pairs across the inner (inner) and the outer (outer) water layer at the end of simulation at a given temperature, in the double bilayers. The number of pairs was averaged over the indicated time period (av. period); errors are standard error estimates. See also Figures 5 and S3–S7.

Water channel formation and transformation

The quadruple bilayer, 2xW15-15 (Figure 4A), consisting of four MGDG bilayers separated by water layers, each containing 15 H_2O/MGDG and initially 11.3 Å wide, was assembled from the last frame of W15-15 simulated for 500 ns. Thus, from the very beginning, in each interface there was one water channel (Figure 4A) and an intensive exchange of MGDG molecules between two outer and two middle leaflets (film Video S2). The bilayer was simulated for 1 μs using semiisotropic pressure control. After ~800 ns (film Video S2) the middle channel, originally along the x axis, closed up and in its place, a new one appeared along the y axis; two other channels transformed into water filled caves (Figures 4C and 4D). The fourth channel between the outer leaflets remained intact (Figure 4C).

In contrast to W15-15, in 2xW15-15 the exchange of MGDG molecules between leaflets continued during the whole simulation. Density profiles across the fragment of the quadruple bilayer where there was no lipid exchange (marked with a *red* rectangle in Figure S8A) and that where there was exchange (marked with a *yellow* rectangle in Figure S8A) were compared in Figures S8B and S8C. In the former case, the density of acyl chains in the interfacial region was zero (Figure S8B); in the latter, it was nonzero (Figure S8C).

Water channel formation and the system size

To ascertain how the formation of water channels depended on the size of the MGDG bilayers in a multibilayer system, the triple bilayer, 6xW15-15-15 (cf. Models), was constructed (Figure 4E) and simulated for 1 μs at 353K (Tables 2 and S1). Its *x* and *y* dimensions were three and two times, respectively, as large as those in the single and double bilayers (Figures 4E–4G). During 1-μs simulation, horizontally water-filled channels that would have extended across the system did not form. Instead, two quite deep caves oriented orthogonally to each other formed. The caves can be seen better in Figure 4G.

Swapping of MGDG molecules

Swapping (exchange) of MGDG molecules across the interface (Figure 6) was a random, local (Figures 7 and S8), concerted, and relatively slow process. It took place in the regions of connected surfaces even though they were not totally dehydrated (~8 H_2O/MGDG). The head group of an MGDG during exchange was H-bonded with 6 ± 2 H_2O molecules (average range 360–460 ns, step 10 ps); also, its acyl chains were exposed to water, as inferred from the radial distribution functions (RDF) of water molecules relative to the chain carbon atoms (Figure 8). The exchange started when the head group protruded further into the interface; this may have happened accidentally as a combined effect of the vertical inter-head attraction and thermal fluctuations (Figures S9A and S9B). The protruding head dragged behind its acyl chains somewhat away from the nonpolar core. At some instance, either the MGDG β (*sn*-2) or the γ (*sn*-1) chain spread across the interface and possibly inserted into the opposite leaflet (Figure S9C); in several cases this resulted in an exchange of the MGDG molecule across the interface. The processes initiated by the MGDG β chain (*blue*) and the γ chain (*yellow*) are shown in films Videos S3 and S4, respectively.

MGDG swapping shown in films Videos S3 and S4 indicate that the initiating chain inserted into and left the opposite leaflet several times without returning to the original one, whereas the other chain left and returned to the original leaflet several times. During exchange, the MGDG molecule resided mainly in the interfacial region, oriented horizontally. When both chains inserted even partially into a leaflet, the whole molecules oriented vertically and both chains embedded deeply into it. However, film Video S5 somehow contradicts this observation—the whole MGDG molecule shown there left and returned to the original leaflet several times. The processes presented in films Videos S3, S4, and S5 lasted ~20, ~100, and ~160 ns, respectively, during which each of the chains assumed different conformations and the extended one was only one of them. The films clearly demonstrate that the swapping process was erratic and dynamic.

Chain splaying—Conformational analysis

To find out which torsion angle was responsible for chain splaying, the time profiles and distributions of torsion angles in the β and the γ chain, as well as the glycerol backbone of three representative MGDG molecules, were calculated. In the case of the β chain, the first of the lipids was

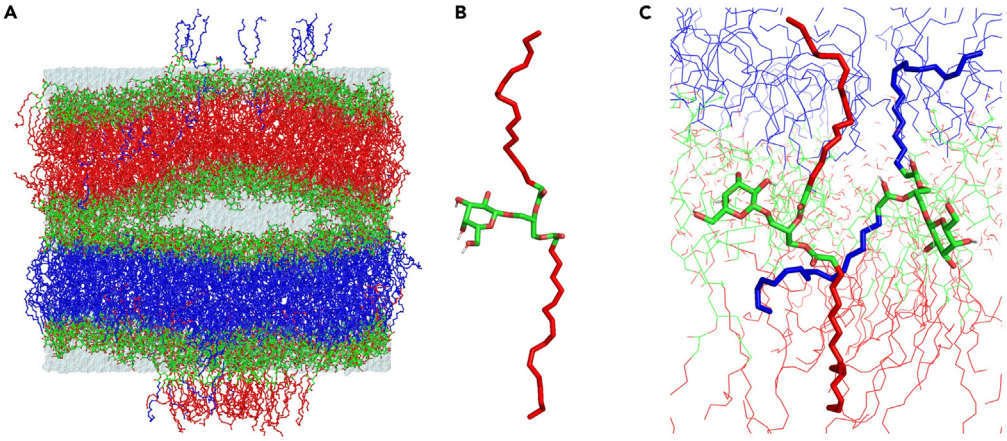

Figure 6. Exchanging of MGDG molecules between leaflets

(A) Snapshot of W15-15 at the end of 1000-ns simulation. Acyl chains are colored *red* for the upper bilayer and *blue* for the lower bilayer to make the exchanging MGDG molecules more visible.

(B) An MGDG molecule from the "*red*" bilayer in the splayed-chain (extended) conformation—it remains in this conformation for 48 ns.

(C) Two simultaneously exchanging MGDG molecules, *red* and *blue*; each is in the extended conformation with chains embedded in the opposing leaflet and head groups in the interface. See also Figures S8 and S9.

from the single MGDG bilayer (*black*), the second was a lipid from W15-15 whose β chain was changing conformation to extended over ∼2 ns (*blue*), and the third was the lipid from W15-15 whose β chain was in a splayed-chain conformation, stable for 48 ns (*red*). The conformations of the first four torsion angles of the β chain and that of the glycerol θ_3 (Figure 1) for the three MGDG molecules determined over 2 ns are compared in Figures S10 and S11.

Kinnunen[14] proposed that the torsion that changed conformation at splaying was of the C(2)-C(3) glycerol bond, i.e., θ_3 in Figure 1. However, conformational analysis reveals a significant difference between the *black* lipid and the *blue* and *red* lipids for the β_3 torsion only (Figures S10–S12). The panels in row 4 of Figure S10 and of Figure S11 indicate that the *black* lipid β_3 oscillated between 180° and 330°, the *red* lipid β_3 oscillated between 60° and 240°, essentially never occupying *gauche*$^-$ conformation, whereas the *blue* lipid β_3 changed conformation from *gauche*$^-$ to *gauche*$^+$ during the first ∼500 ps of the analysis time and then for the remaining 1500 ps oscillated within a similar range to that of the *red* lipid, i.e., ∼60°–200°, again, never occupying the *gauche*$^-$ conformation. However, the actual transition from *gauche*$^-$ to *gauche*$^+$ was much faster and took place within ∼9 ps (Figure S13). The difference between the conformations of β_3 torsion of the *black* and the *red* lipid is especially apparent in Figure S12, where the distributions of the torsion angles over 100-ns (*black*) and 48-ns (*red*) analyses are compared. Unfortunately, a longer analysis for the *blue* lipid β chain was not possible because its continuous splayed-chain conformation lasted only ∼2 ns.

A similar comparative analysis was performed for the γ chains of selected MGDG molecules. The time profiles and distributions of γ chain torsion angles recorded over 2 ns are compared in Figures S14 and S15, respectively, for three MGDG molecules, one from the single MGDG bilayer (*black*), another from W15-15 whose γ chain was changing conformation to extended (*green*), and the other was the *blue* MGDG from Figures S10 and S11 whose β chain was changing conformation to extended (*blue*). As in the case of the β chain, the significant differences in the profiles and distributions were for the γ_3 only (Figures S14 and S15).

Concerted MGDG swapping

The analyses in Refs.[27,28] indicate that insertion of an acyl chain of one phospholipid into the bilayer interface triggered other lipids to follow, which resulted in the formation of a stalk. In simulations of W15-15 and 2xW15-15 a similar triggering was observed, although MGDG molecules did not form a "classic" stalk but located in one of the opposing leaflets. The concerted exchange of several MGDG molecules started in W15-15 at ∼350 ns of simulation but at ∼900 ns the exchange slowed down (film Video S1). In 2xW15-15 it lasted for the whole simulation (film Video S2). An example of a synchronized swapping of a chosen pair of MGDG molecules is shown in film Video S6.

Effect of pressure control algorithm

To make a comparison of the behavior of systems simulated with a semiisotropic and an anisotropic barostat (cf. STAR Methods) easier, new names were given to these systems (Table 4). In Table 4, the effects of the chosen pressure control algorithm are also summarized.

The pressure control algorithm used in these simulations had a significant effect on the systems' behavior and stability (Table 4). As already noted, simulations of the systems at 295 K (Table 1) using an anisotropic barostat did not introduce any distortion of the dimensions of the systems relative to the initial ones. At 333 and 353 K in some systems one of the dimensions increased and the other shrank. To enable comparison and evaluation of the behavior of all systems, the systems that distorted at higher temperatures were resimulated (Table 4) and others

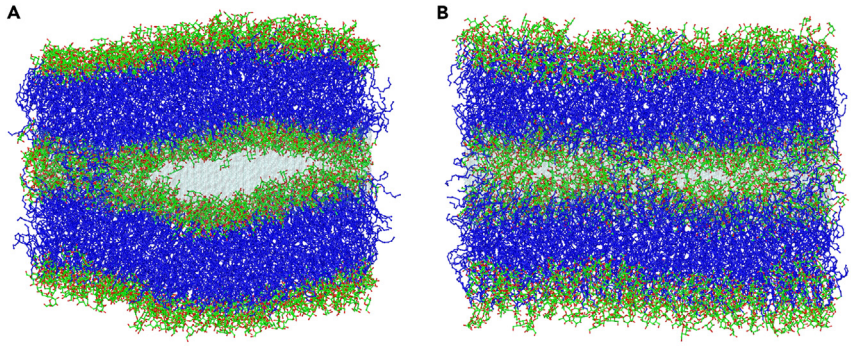

Figure 7. Local exchange of MGDG molecules across the interface

(A and B) The (A) front and (B) side view of the outer leaflets of 2xW15-15. Both in (A) and (B) acyl chains of several MGDG molecules can be seen in the interfacial region. Other details as in Figure 2. See also Figure S8.

(Table 2) were simulated with a semiisotropic barostat. Anisotropic-pressure-induced change of the box-length proportions somehow facilitated formation and stability of the water channels. Finding a correlation between the MGDG bilayer compulsion to form stalks and channels and a pressure-induced change of the system dimensions that enabled these formations and proposing a putative driving force behind such behavior are beyond the scope of this paper. However, it was interesting to compare W15-30_semi and W15-30_ani (Table 4). The final enlarged structures of the systems are compared in Figures S16B and S16D. When the proportions of the simulation box were preserved, there was no water channel in the middle layer of W15-30_semi; this is because the bilayers could not bend sufficiently to close the tube with the accumulated "free" water (Figure S16B). When the system lengthened, to close the tube a smaller curvature of the bilayers was required, so the second water channel with the vertical cross-section of a flattened ellipse was formed (Figure S16D). Similar reasoning as to why the water channels in 2xW15-15_ani were more stable than in 2xW15-15_semi could probably be offered, but this would not convincingly explain other cases, thus the effect of anisotropic pressure control was classified as "unpredictable".

DISCUSSION

Molecular modeling with atomic resolution allows the behavior of molecules to be studied on a much shorter timescale than that with coarse-grained resolution. Nevertheless, it provides a much deeper insight into molecular and atomic level mechanisms, leading to certain behavior of the molecules. The simulations carried out in this study were long enough to capture, step by step, events leading to spontaneous formation of a hexagonal-like lattice of water channels in stacks of hydrated MGDG bilayers. The formation and the number of water channels depend predominantly on the widths of the water layers separating the bilayers. The results obtained for double bilayers that have 15 × 15 MGDG molecules in each leaflet indicate that a water channel forms when the width of the inner water layer is not smaller than ∼10 Å and significantly smaller than ∼23 Å, whereas that of the outer layer is larger than ∼10 Å. When the widths of both water layers are ∼10 Å, then two water channels develop, and when one width is ∼10 Å and the other is ∼23 Å, only one channel develops. When these conditions are fulfilled, the two bilayers bend locally in opposite directions and create a space where the inter-bilayer unbound to MGDG water molecules can accumulate. To complete the channel formation, the accumulated water has to be sealed in a tube; this can happen only when other fragments of the bilayers, either oppositely curved or flat (cf. Figure S16D), but certainly poorly hydrated, come into close contact, enabling numerous vertical lipid-lipid connections to be made. Otherwise, the channel is not created. Both a situation where a channel is created and one where it is not are depicted in Figure S16B, where W15-30_semi (Table 4) is graphically enlarged in the *x*- and *z*-direction by translating the simulation box. In each of the outer layers, two channels are fully created, whereas in the middle one no channel could form because sealing the accumulated water in a tube would require too much bending of the bilayers due to the large width of the water layer.

However, not only the widths of the water layers separating the bilayers in a multibilayer system but also the system size and shape have an impact on the formation and stability of the water channels. The former is exemplified by 6xW15-15-15, consisting of three bilayers (2 × 45×30 MGDG molecules each), initially separated by ∼11 Å-wide water layers. Even though such a width is sufficient for water channels to form in W15-15 and 2xW15-15, in the system consisting of bilayers that are six times as large, no channel forms. During 1-μs simulation only deep caves between bilayers develop (Figures 4E and 4F).

The effect of the system shape is exemplified by W15-30_ani and 2xW15-15_ani (Table 4; Figures S16C, S16D, and S17). Their horizontal cross-section is originally a square. Due to pressure anisotropy it changes to an elongated rectangle of the same area, thus the widths of the water layers in the systems remain unchanged. Nevertheless, in W15-30_ani the second channel emerges, and in 2xW15-15_ani the channels are stable, even though this is not the case in W15-30_semi and 2xW15-15_semi.

These results agree with the common-sense assumption that the development of a water channel in a multibilayer system requires a large reorganization of the system and cooperative action of MGDG molecules. Thus this should depend on the overall size of the bilayers and the proportion of their dimensions. When one bilayer side is significantly narrower than the other (in the case of W15-30_ani the proportion is ∼25:5 nm), cooperativity is easier to achieve; this notion is backed by the formation of the second channel in W15-30_ani but not in W15-30_semi. It is then quite likely that the completion of the channel formation in 6xW15-15-15 simply needs more time than 1 μs.

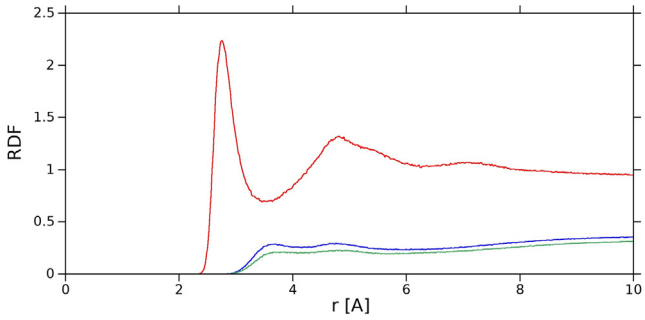

Figure 8. Hydration of a MGDG molecule during swapping

RDFs of water molecules relative to the MGDG β-chain (*blue*) and γ-chain (*green*) carbon atoms and head group oxygen atoms (*red*) of an MGDG molecule during swapping between leaflets.

Instability but not disappearance of the channels in 2xW15-15_semi illustrates both the propensity of MGDG bilayers to bend and the highly dynamic character of the lipid systems, as not only vertical MGDG connections continually form and break but also water channels can locally disappear to appear in a different location or temporally transform into water-filled caves. Nevertheless, the formation of a channel is not a reversible process.

The result that ~15 H_2O/MGDG is needed for a water channel to develop between two MGDG bilayers apparently concurs with the experimental results obtained for the MGDG H_{II} phase where the number of H_2O/MGDG was estimated as ~12–13[5] and 14.[58] However, the actual number of H_2O/MGDG inside the water channel estimated here as 18.8 ± 0.3 is larger than that estimated experimentally[5,58] and smaller than 30 H_2O/MGDG in each water channel of the MGDG H_{II} phase generated in our previous study.[49]

The effect of bilayer hydration on the connected surface (stalk) formation between MGDG bilayers in a double bilayer revealed in this atomistic (AA) simulation somewhat disagrees with that revealed in the coarse-grained (CG) simulation of the dioleoylPE (DOPE) multibilayer at 308 K.[59] In that CG simulation, no stalk formed at hydration higher than 12 H_2O/DOPE, whereas in this AA simulation, vertical MGDG connections (stalks) formed at hydration up to 15 H_2O/MGDG at both 295 and 333 K. Connections did not form when hydration was 30 H_2O/MGDG at 353 K. The difference between the two systems arises presumably from much stronger cross-interface links between MGDG head groups than between DOPE head groups and a higher negative intrinsic curvature of MGDG. Nevertheless, none of the MGDG multibilayer systems investigated in this study converted to the H_{II} phase, which was the case in the CG simulation.[59]

Protrusion of phospholipid acyl chains out of the bilayer hydrophobic core as well as induced or spontaneous exchange of lipid molecules between apposing leaflets triggered by local "manual" dehydration of the bilayer leaflets were observed in previous computer simulation studies using AA[60] and CG[27,28] lipid and water models. The CG simulations indicate that lipid exchange proceeded via the splayed-chain conformation.

This AA simulation study, carried out over a much longer timescale than in Ref.[60], captures subsequent steps of lipid exchange between apposing bilayer leaflets. The exchange occurs locally, even though vertical MGDG pairs form over the large area of the adjacent leaflets. In general, the process of MGDG exchange over the interface proceeds similarly to that of phospholipids shown in CG simulations;[27,28] however, there are two substantial differences between them. First, in the MGDG systems dehydration of connected fragments of opposing leaflets is spontaneous due to bilayer bending, which allows for the local accumulation of "free" bilayer water and significant dehydration of other bilayer surfaces. Second, even though the swapping of MGDG molecules between adjacent leaflets proceeds mainly via splaying of lipid chains, and swapping is a concerted process, the lipids do not form a stable "classic" semi-toroidal stalk, but instead they locate eventually in one of the facing leaflets.

This study also reveals that the torsion angle that drastically changes during chain transition to the extended conformation is either β_3 or γ_3, depending on which of the MGDG chains initiates exchange of the molecule. Thus, the torsion that changes conformation at splaying is not θ_3, as suggested by Kinnunen.[14] Moreover, contrary to the speculation of Corkery[26] that the *sn*-2 acyl chain (β) of a native phospholipid has a higher probability to extend than the *sn*-1 chain (γ), these simulations indicate that, on the basis of 15 cases, the probability of the extended conformation is almost the same for the β and the γ chain of MGDG. However, phospholipids generally have only one mono-*cis*-unsaturated chain (β), whereas both chains of MGDG are triple-*cis*-unsaturated, and this is the possible cause of the difference.

Experimental studies on model thylakoid membranes presented in Ref.[20] show that MGDG and DGDG directly contribute to stacking of thylakoids into grana and that thylakoid membranes are locally linked by stalks. Our present and previous[50] results strongly support these experimental findings by demonstrating that the head groups of MGDG and DGDG[50] form strong and numerous short-range interactions. Moreover, in the case of MGDG bilayers, these interactions take place across the bilayer interfacial region. It is rational to suppose that between the aligned mixed MGDG-DGDG bilayers cross-interface connections are even stronger.

Spontaneous formation of water channels between stacked MGDG bilayers is in line with experimental results that the H_{II} phase is necessary for the xanthophyll cycle to occur,[38–40] but then the H_{II} phase should not be understood as a structure with a long-range orientational order but locally formed water-filled cylindrical structures. Such structures were able to emerge when, under a certain condition, lipids constituting thylakoid membranes segregated locally into lateral domains and MGDG domains in adjacent leaflets came into close contact. Most

Table 4. Names and structural parameters of systems simulated with different pressure control algorithm

System name	Temperature [K]	Pressure control	Simulation time [ns]	Final effect
W8-30_semi	353	semi	500	No channel; *x*, *y* preserved
W8-30_ani	353	ani	500	No channel; *x* extended, *y* shrank
W15-30_semi	333	semi	500	One stable channel; *x*, *y* preserved
W15-30_ani	333	ani	1400	Two unequal stable channels; *x* extended, *y* shrank
2xW15-15_semi	353	semi	1000	Four unstable channels; *x*, *y* preserved
2xW15-15_ani	353	ani/semi	170 ani/900 semi	Four stable asymmetrically distributed channels; *x* extended, *y* shrank

(semi) indicates a semiisotropic and (ani) indicates an anisotropic barostat. *x*, *y* are the in-plane dimensions of the simulation box. See also Figures S16 and S17.

likely, two domains facing each other would behave similarly to a model MGDG double bilayer, that is, form a hexagonal-like lattice of water channels.

The results obtained in this study and those published in the literature are combined in Table 5 in order to summarize them and to make the comparison easier.

Limitations of the study

This MD simulation study was carried out with force field parameters for the MGDG and water molecules that were verified in several previous studies[45,47–50] and with simulation parameters recommended in the GROMACS User Manual. This, together with the quite conventional methodology employed, should give confidence that the results of the study are reasonable. Furthermore, it should be rather straightforward to perform similar calculations of similar systems.

The processes modeled here have not been investigated with atomic resolution so far, so during the study unexpected effects were encountered. We did not foresee that some of the results would depend on such factors as the effect of the pressure control algorithm or the shape and size of the simulation box. To avoid false conclusions, simulations were carried out using both a semiisotropic and anisotropic barostat. In some cases, the latter had an effect on the shape of the simulation box, which resulted in a different evolution of the simulated system compared with that simulated using a semiisotropic barostat, which maintained the box proportions. The conclusions presented in discussion were drawn on the basis of the results obtained for the systems where box proportions were preserved relative to the initial ones; this enabled general conclusions to be drawn. However, it turned out that the conclusions derived for smaller systems could not be straightforwardly extended on a much larger system, even though it was simulated for a similar time; this is most likely because in larger systems reorganization processes take more time to complete than in smaller ones.

STAR★METHODS

Detailed methods are provided in the online version of this paper and include the following:

- KEY RESOURCES TABLE
- RESOURCE AVAILABILITY
  - Lead contact
  - Materials availability
  - Data and code availability
- METHOD DETAILS
  - Simulation parameters and conditions
- QUANTIFICATION AND STATISTICAL ANALYSIS

SUPPLEMENTAL INFORMATION

Supplemental information can be found online at https://doi.org/10.1016/j.isci.2023.107863.

ACKNOWLEDGMENTS

We gratefully acknowledge the Polish high-performance computing infrastructure PLGrid (HPC Centers: ACK Cyfronet AGH) for providing computer facilities and support within computational grant no. PLG/2022/015999. Some calculations were performed under the Project HPC-EUROPA3 (INFRAIA-2016-1–730,897), with the support of EC Research Innovation Action under the H2020 Programme. J.H. acknowledges the support of the project for PhD students and Young Scientists FBBB N19/MNW/000014 as well as the support of Waldemar Kulig, University of Helsinki and the resources and technical support provided by CSC. M.P.G. thanks K. Strzalka for inspiring discussions. The open-

Table 5. Summary and comparison of the results of this study and those published in the literature

Result	This simulation study, AA MGDG, and water models	Literature
H_{II} phase formation	No, only connected surfaces (stalks) and water channels	Yes, CG DOPE and water models[59] No, CG POPC and water models[27] No, CG PC, PE, and water models[28]
Spontaneous local dehydration of the bilayer surface	Yes	Yes, CG DOPE and water models[59] No, CG POPC and water models[27] No, CG PC, PE and water models[28]
"Classic" stalk formation	No, MGDG only exchanges across the interface	Yes, CG simulation[59] Yes, CG simulation[27]
Number (#) of H_2O/MGDG needed to form a water channel or H_{II} phase	Water channel: 15 H_2O/MGDG, (estimated #H_2O/MGDG inside a water channel ~18.8 ± 0.3)	H_{II} phase: 12-13 H_2O/MGDG, X-ray[5] 14 H_2O/MGDG, NMR[58] 12 H_2O/MGDG, CG simulation[59]
Exchange of lipids between apposing leaflets	Yes, local, mainly via splayed-chain	Yes, local, via splayed-chain[27,28]
Probability, which of the acyl chains of a lipid molecule splays	Almost the same for the β and γ chain of MGDG	Higher probability of *sn*-2 (β) chain of a natural phospholipid[26]
Torsion responsible for chain splaying	The third torsion (β3 or γ3) of the chain initiating splaying	Glycerol backbone θ3[14]

access publication of this article was funded by the Department of Computational Biophysics and Bioinformatics, Jagiellonian University, Krakow, Poland.

AUTHOR CONTRIBUTIONS

J.H. built models, performed MD simulations and analyses, prepared figures; M.M. supervised J.H. work; M.P-G conceived and supervised the research and wrote and revised the manuscript with contributions from all authors.

DECLARATION OF INTERESTS

The authors declare no competing interests.

Received: June 1, 2023
Revised: August 17, 2023
Accepted: September 6, 2023
Published: September 9, 2023

REFERENCES

1. Dörmann, P., and Benning, C. (2002). Galactolipids rule in seed plants. Trends Plant Sci. *7*, 112–118. https://doi.org/10.1016/s1360-1385(01)02216-6.
2. Kobayashi, K. (2016). Role of membrane glycerolipids in photosynthesis, thylakoid biogenesis and chloroplast development. J. Plant Res. *129*, 565–580. https://doi.org/10.1007/s10265-016-0827-y.
3. Ohlrogge, J., and Browse, J. (1995). Lipid biosynthesis. Plant Cell *7*, 957–970. https://doi.org/10.1105/tpc.7.7.957.
4. Lee, A.G. (2000). Membrane lipids: it's only a phase. Curr. Biol. *10*, R377–R380. https://doi.org/10.1016/s0960-9822(00)00477-2.
5. Shipley, G.G., Green, J.P., and Nichols, B.W. (1973). The phase behavior of monogalactosyl, digalactosyl, and sulphoquinovosyl diglycerides. Biochim. Biophys. Acta *311*, 531–544. https://doi.org/10.1016/0005-2736(73)90128-4.
6. Simidjiev, I., Stoylova, S., Amenitsch, H., Javorfi, T., Mustardy, L., Laggner, P., Holzenburg, A., and Garab, G. (2000). Self-assembly of large, ordered lamellae from non-bilayer lipids and integral membrane proteins *in vitro*. Proc. Natl. Acad. Sci. USA *97*, 1473–1476. https://doi.org/10.1073/pnas.97.4.1473.
7. Luzzati, V., and Husson, F. (1962). Structure of Liquid-Crystalline Phases of Lipid-Water Systems. J. Cell Biol. *12*, 207–219. https://doi.org/10.1083/jcb.12.2.207.
8. Seddon, J.M. (1990). Structure of the inverted hexagonal (HII) phase, and non-lamellar phase transitions of lipids. Biochim. Biophys. Acta *1031*, 1–69. https://doi.org/10.1016/0304-4157(90)90002-t.
9. Siegel, D.P., and Epand, R.M. (1997). The mechanism of lamellar-to-inverted hexagonal phase transitions in phosphatidylethanolamine: Implications for membrane fusion mechanisms. Biophys. J. *73*, 3089–3111. https://doi.org/10.1016/S0006-3495(97)78336-X.
10. Rappolt, M., Hickel, A., Bringezu, F., and Lohner, K. (2003). Mechanism of the lamellar/inverse hexagonal phase transition examined by high resolution x-ray diffraction. Biophys. J. *84*, 3111–3122. https://doi.org/10.1016/S0006-3495(03)70036-8.
11. Kinnunen, P.K., and Holopainen, J.M. (2000). Mechanisms of initiation of membrane fusion: Role of lipids. Biosci. Rep. *20*, 465–482. https://doi.org/10.1023/A:1010402819509.
12. Markin, V.S., Kozlov, M.M., and Borovjagin, V.L. (1984). On the Theory of Membrane-Fusion - the Stalk Mechanism. Gen. Physiol. Biophys. *3*, 361–377.
13. Siege, D.P. (1987). Membrane-Membrane Interactions via Intermediates in Lamellar-to-Inverted Hexagonal Phase Transitions. In Cell

Fusion, A.E. Sowers, ed. (Springer), pp. 181–207.
14. Kinnunen, P.K. (1992). Fusion of Lipid Bilayers - a Model Involving Mechanistic Connection to Hii-Phase Forming Lipids. Chem. Phys. Lipids *63*, 251–258. https://doi.org/10.1016/0009-3084(92)90041-M.
15. Khattari, Z., Köhler, S., Xu, Y., Aeffner, S., and Salditt, T. (2015). Stalk formation as a function of lipid composition studied by X-ray reflectivity. Biochim. Biophys. Acta *1848*, 41–50. https://doi.org/10.1016/j.bbamem.2014.08.010.
16. Salditt, T., and Aeffner, S. (2016). X-ray structural investigations of fusion intermediates: Lipid model systems and beyond. Semin. Cell Dev. Biol. *60*, 65–77. https://doi.org/10.1016/j.semcdb.2016.06.014.
17. Markin, V.S., and Albanesi, J.P. (2002). Membrane fusion: Stalk model revisited. Biophys. J. *82*, 693–712. https://doi.org/10.1016/S0006-3495(02)75432-5.
18. Kozlov, M.M., Leikin, S.L., Chernomordik, L.V., Markin, V.S., and Chizmadzhev, Y.A. (1989). Stalk mechanism of vesicle fusion. Intermixing of aqueous contents. Eur. Biophys. J. *17*, 121–129. https://doi.org/10.1007/BF00254765.
19. Siegel, D.P. (1993). Energetics of Intermediates in Membrane-Fusion - Comparison of Stalk and Inverted Micellar Intermediate Mechanisms. Biophys. J. *65*, 2124–2140. https://doi.org/10.1016/S0006-3495(93)81256-6.
20. Seiwert, D., Witt, H., Ritz, S., Janshoff, A., and Paulsen, H. (2018). The Nonbilayer Lipid MGDG and the Major Light-Harvesting Complex (LHCII) Promote Membrane Stacking in Supported Lipid Bilayers. Biochemistry *57*, 2278–2288. https://doi.org/10.1021/acs.biochem.8b00118.
21. Aeffner, S., Reusch, T., Weinhausen, B., and Salditt, T. (2012). Energetics of stalk intermediates in membrane fusion are controlled by lipid composition. Proc. Natl. Acad. Sci. *109*, E1609–E1618. https://doi.org/10.1073/pnas.1119442109.
22. McNew, J.A., Parlati, F., Fukuda, R., Johnston, R.J., Paz, K., Paumet, F., Söllner, T.H., and Rothman, J.E. (2000). Compartmental specificity of cellular membrane fusion encoded in SNARE proteins. Nature *407*, 153–159. https://doi.org/10.1038/35025000.
23. Xu, Y., Kuhlmann, J., Brennich, M., Komorowski, K., Jahn, R., Steinem, C., and Salditt, T. (2018). Reconstitution of SNARE proteins into solid-supported lipid bilayer stacks and X-ray structure analysis. BBA-Biomembr. *1860*, 566–578. https://doi.org/10.1016/j.bbamem.2017.10.023.
24. Han, J., Pluhackova, K., and Böckmann, R.A. (2017). The Multifaceted Role of SNARE Proteins in Membrane Fusion. Front. Physiol. *8*. ARTN 5. https://doi.org/10.3389/fphys.2017.00005.
25. Cullis, P.R., and de Kruijff, B. (1979). Lipid polymorphism and the functional roles of lipids in biological membranes. Biochim. Biophys. Acta *559*, 399–420. https://doi.org/10.1016/0304-4157(79)90012-1.
26. Corkery, R.W. (2002). The anti-parallel, extended or splayed-chain conformation of amphiphilic lipids. Colloids Surf., B *26*, 3–20. https://doi.org/10.1016/S0927-7765(02)00034-6.
27. Smirnova, Y.G., Marrink, S.J., Lipowsky, R., and Knecht, V. (2010). Solvent-Exposed Tails as Prestalk Transition States for Membrane Fusion at Low Hydration. J. Am. Chem. Soc. *132*, 6710–6718. https://doi.org/10.1021/ja910050x.
28. Mirjanian, D., Dickey, A.N., Hoh, J.H., Woolf, T.B., and Stevens, M.J. (2010). Splaying of Aliphatic Tails Plays a Central Role in Barrier Crossing During Liposome Fusion. J. Phys. Chem. B *114*, 11061–11068. https://doi.org/10.1021/jp1055182.
29. Holopainen, J.M., Lehtonen, J.Y., and Kinnunen, P.K. (1999). Evidence for the extended phospholipid conformation in membrane fusion and hemifusion. Biophys. J. *76*, 2111–2120. https://doi.org/10.1016/S0006-3495(99)77367-4.
30. Scheidt, H.A., Kolocaj, K., Konrad, D.B., Frank, J.A., Trauner, D., Langosch, D., and Huster, D. (2020). Light-induced lipid mixing implies a causal role of lipid splay in membrane fusion. BBA-Biomembr. *1862*, 183438. https://doi.org/10.1016/j.bbamem.2020.183438.
31. Agre, P. (2006). The aquaporin water channels. Proc. Am. Thorac. Soc. *3*, 5–13. https://doi.org/10.1513/pats.200510-109JH.
32. Lim, Y.J., Goh, K., and Wang, R. (2022). The coming of age of water channels for separation membranes: from biological to biomimetic to synthetic. Chem. Soc. Rev. *51*, 4537–4582. https://doi.org/10.1039/d1cs01061a.
33. Szilágyi, A., Sommarin, M., and Akerlund, H.E. (2007). Membrane curvature stress controls the maximal conversion of violaxanthin to zeaxanthin in the violaxanthin cycle - influence of alpha-tocopherol, cetylethers, linolenic acid, and temperature. BBA-Biomembr. *1768*, 2310–2318. https://doi.org/10.1016/j.bbamem.2007.06.001.
34. Szilágyi, A., Selstam, E., and Akerlund, H.E. (2008). Laurdan fluorescence spectroscopy in the thylakoid bilayer: The effect of violaxanthin to zeaxanthin conversion on the galactolipid dominated lipid environment. BBA-Biomembr. *1778*, 348–355. https://doi.org/10.1016/j.bbamem.2007.10.006.
35. Rast, A., Heinz, S., and Nickelsen, J. (2015). Biogenesis of thylakoid membranes. BBA-Bioenerg. *1847*, 821–830. https://doi.org/10.1016/j.bbabio.2015.01.007.
36. Garab, G., Ughy, B., Waard, P.d., Akhtar, P., Javornik, U., Kotakis, C., Šket, P., Karlický, V., Materová, Z., Špunda, V., et al. (2017). Lipid polymorphism in chloroplast thylakoid membranes - as revealed by (31)P-NMR and time-resolved merocyanine fluorescence spectroscopy. Sci. Rep. *7*, 13343. https://doi.org/10.1038/s41598-017-13574-y.
37. Armbruster, U., Labs, M., Pribil, M., Viola, S., Xu, W., Scharfenberg, M., Hertle, A.P., Rojahn, U., Jensen, P.E., Rappaport, F., et al. (2013). Arabidopsis CURVATURE THYLAKOID1 proteins modify thylakoid architecture by inducing membrane curvature. Plant Cell *25*, 2661–2678. https://doi.org/10.1105/tpc.113.113118.
38. Latowski, D., Akerlund, H.E., and Strzałka, K. (2004). Violaxanthin de-epoxidase, the xanthophyll cycle enzyme, requires lipid inverted hexagonal structures for its activity. Biochemistry *43*, 4417–4420. https://doi.org/10.1021/bi049652g.
39. Goss, R., Lohr, M., Latowski, D., Grzyb, J., Vieler, A., Wilhelm, C., and Strzalka, K. (2005). Role of hexagonal structure-forming lipids in diadinoxanthin and violaxanthin solubilization and de-epoxidation. Biochemistry *44*, 4028–4036. https://doi.org/10.1021/bi047464k.
40. Goss, R., and Latowski, D. (2020). Lipid Dependence of Xanthophyll Cycling in Higher Plants and Algae. Front. Plant Sci. *11*, 455. https://doi.org/10.3389/fpls.2020.00455.
41. López, C.A., Sovova, Z., van Eerden, F.J., de Vries, A.H., and Marrink, S.J. (2013). Martini Force Field Parameters for Glycolipids. J. Chem. Theory Comput. *9*, 1694–1708. https://doi.org/10.1021/ct3009655.
42. van Eerden, F.J., de Jong, D.H., de Vries, A.H., Wassenaar, T.A., and Marrink, S.J. (2015). Characterization of thylakoid lipid membranes from cyanobacteria and higher plants by molecular dynamics simulations. Biochim. Biophys. Acta *1848*, 1319–1330. https://doi.org/10.1016/j.bbamem.2015.02.025.
43. Makshakova, O., Breton, C., and Perez, S. (2020). Unraveling the complex enzymatic machinery making a key galactolipid in chloroplast membrane: a multiscale computer simulation. Sci. Rep. *10*, 13514. https://doi.org/10.1038/s41598-020-70425-z.
44. Chng, C.P., Wang, K., Ma, W., Hsia, K.J., and Huang, C. (2022). Chloroplast membrane lipid remodeling protects against dehydration by limiting membrane fusion and distortion. Plant Physiol. *188*, 526–539. https://doi.org/10.1093/plphys/kiab512.
45. Baczynski, K., Markiewicz, M., and Pasenkiewicz-Gierula, M. (2015). A computer model of a polyunsaturated monogalactolipid bilayer. Biochimie *118*, 129–140. https://doi.org/10.1016/j.biochi.2015.09.007.
46. Baczynski, K., Markiewicz, M., and Pasenkiewicz-Gierula, M. (2018). Is the tilt of the lipid head group correlated with the number of intermolecular interactions at the bilayer interface? FEBS Lett. *592*, 1507–1515. https://doi.org/10.1002/1873-3468.13048.
47. Markiewicz, M., Baczyński, K., and Pasenkiewicz-Gierula, M. (2015). Properties of water hydrating the galactolipid and phospholipid bilayers: a molecular dynamics simulation study. Acta Biochim. Pol. *62*, 475–481. https://doi.org/10.18388/abp.2015_1077.
48. Szczelina, R., Baczynski, K., Markiewicz, M., and Pasenkiewicz-Gierula, M. (2020). Network of lipid interconnections at the interfaces of galactolipid and phospholipid bilayers. J. Mol. Liq. *298*, 112002. https://doi.org/10.1016/j.molliq.2019.112002.
49. Bratek, L., Markiewicz, M., Baczynski, K., Jalocha-Bratek, J., and Pasenkiewicz-Gierula, M. (2019). Inverse hexagonal phase of poly-unsaturated monogalactolipid: A computer model and analysis. J. Mol. Liq. *290*, 111189. https://doi.org/10.1016/j.molliq.2019.111189.
50. Hryc, J., Szczelina, R., Markiewicz, M., and Pasenkiewicz-Gierula, M. (2022). Lipid/water interface of galactolipid bilayers in different lyotropic liquid-crystalline phases. Front. Mol. Biosci. *9*, 958537. https://doi.org/10.3389/fmolb.2022.958537.
51. Jouhet, J. (2013). Importance of the hexagonal lipid phase in biological membrane organization. Front. Plant Sci. *4*, 494. https://doi.org/10.3389/fpls.2013.00494.
52. Kowalewska, Ł., Bykowski, M., and Mostowska, A. (2019). Spatial organization of thylakoid network in higher plants. Bot. Lett. *166*, 326–343. https://doi.org/10.1080/23818107.2019.1619195.
53. Garab, G., Yaguzhinsky, L.S., Dlouhý, O., Nesterov, S.V., Špunda, V., and Gasanoff, E.S. (2022). Structural and functional roles of

non-bilayer lipid phases of chloroplast thylakoid membranes and mitochondrial inner membranes. Prog. Lipid Res. *86*, 101163. https://doi.org/10.1016/j.plipres.2022.101163.

54. Koltover, I., Salditt, T., Rädler, J.O., and Safinya, C.R. (1998). An inverted hexagonal phase of cationic liposome-DNA complexes related to DNA release and delivery. Science *281*, 78–81. https://doi.org/10.1126/science.281.5373.78.
55. Sundaralihgam, M. (1972). Discussion Paper: Molecular Structures and Conformations of the Phospholipids and Sphingomyelins. Ann. N. Y. Acad. Sci. *195*, 324–355. https://doi.org/10.1111/j.1749-6632.1972.tb54814.x.
56. McNaught, A.D. (1996). Nomenclature of carbohydrates (IUPAC recommendations 1996). Pure Appl. Chem. *68*, 1919–2008.
57. Allouche, A.-r. (2011). Software News and Updates Gabedit — A Graphical User Interface for Computational Chemistry Softwares. J. Comput. Chem. *32*, 174–182. https://doi.org/10.1002/jcc.
58. Brentel, I., Selstam, E., and Lindblom, G. (1985). Phase-Equilibria of Mixtures of Plant Galactolipids - the Formation of a Bicontinuous Cubic Phase. Biochim. Biophys. Acta *812*, 816–826. https://doi.org/10.1016/0005-2736(85)90277-9.
59. Marrink, S.J., and Mark, A.E. (2004). Molecular view of hexagonal phase formation in phospholipid membranes. Biophys. J. *87*, 3894–3900. https://doi.org/10.1529/biophysj.104.048710.
60. Ohta-Iino, S., Pasenkiewicz-Gierula, M., Takaoka, Y., Miyagawa, H., Kitamura, K., and Kusumi, A. (2001). Fast lipid disorientation at the onset of membrane fusion revealed by molecular dynamics simulations. Biophys. J. *81*, 217–224. https://doi.org/10.1016/S0006-3495(01)75693-7.
61. Abraham, M.J., Murtola, T., Schulz, R., Páll, S., Smith, J.C., Hess, B., and Lindahl, E. (2015). GROMACS: High performance molecular simulations through multi-level parallelism from laptops to supercomputers. SoftwareX *1–2*, 19–25. https://doi.org/10.1016/j.softx.2015.06.001.
62. Humphrey, W., Dalke, A., and Schulten, K. (1996). VMD: Visual molecular dynamics. J. Mol. Graph. *14*, 33-8–27-8. https://doi.org/10.1016/0263-7855(96)00018-5.
63. DeLano, W. (2010). The PyMOL Molecular Graphics System 1.8.4.
64. Williams, T., and Kelley, C. (2017). Gnuplot 5.2 Manual: An Interactive Plotting Program (12th Media Services).
65. Aho, A.V., Kernighan, B.W., and Weinberger, P.J. (1988). The AWK Programming Language (Addison-Wesley).
66. Damm, W., Frontera, A., TiradoRives, J., and Jorgensen, W.L. (1997). OPLS all-atom force field for carbohydrates. J. Comput. Chem. *18*, 1955–1970. https://doi.org/10.1002/(Sici)1096-987x(199712)18:16<1955::Aid-Jcc1>3.0.Co;2-L.
67. Maciejewski, A., Pasenkiewicz-Gierula, M., Cramariuc, O., Vattulainen, I., and Rog, T. (2014). Refined OPLS all-atom force field for saturated phosphatidylcholine bilayers at full hydration. J. Phys. Chem. B *118*, 4571–4581. https://doi.org/10.1021/jp5016627.
68. Essmann, U., Perera, L., Berkowitz, M.L., Darden, T., Lee, H., and Pedersen, L.G. (1995). A Smooth Particle Mesh Ewald Method. J. Chem. Phys. *103*, 8577–8593. https://doi.org/10.1063/1.470117.
69. Berendsen, H.J.C., Postma, J.P.M., Vangunsteren, W.F., Dinola, A., and Haak, J.R. (1984). Molecular-Dynamics with Coupling to an External Bath. J. Chem. Phys. *81*, 3684–3690. https://doi.org/10.1063/1.448118.
70. Nosé, S. (1984). A unified formulation of the constant temperature molecular dynamics methods. J. Chem. Phys. *81*, 511–519. https://doi.org/10.1063/1.447334.
71. Parrinello, M., and Rahman, A. (1981). Polymorphic Transitions in Single-Crystals - a New Molecular-Dynamics Method. J. Appl. Phys. *52*, 7182–7190. https://doi.org/10.1063/1.328693.
72. Hess, B., Bekker, H., Berendsen, H.J.C., and Fraaije, J.G.E.M. (1997). LINCS: A linear constraint solver for molecular simulations. J. Comput. Chem. *18*, 1463–1472. https://doi.org/10.1002/(Sici)1096-987x(199709)18:12<1463::Aid-Jcc4>3.0.Co;2-H.
73. Project, I. (2020). Inkscape: Draw Freely.

STAR★METHODS

KEY RESOURCES TABLE

REAGENT or RESOURCE	SOURCE	IDENTIFIER
Software and algorithms		
GROMACS 5.05 software package	Abraham et al.[61]	https://www.gromacs.org/
VMD 1.9.3	Humphrey et al.[62]	https://www.ks.uiuc.edu/Research/vmd/
PyMOL 1.8.4	DeLano[63]	https://pymol.org/2/
Gnuplot	Williams et al.[64]	http://www.gnuplot.info/
AWK	Aho et al.[65]	https://www.gnu.org/software/gawk/manual/gawk.html

RESOURCE AVAILABILITY

Lead contact

Further information and requests for resources and reagents should be directed to, and will be fulfilled, by the lead contact, Jakub Hryc (jakub.hryc@uj.edu.pl).

Materials availability

This study did not generate new unique reagents.

Data and code availability

- All data reported in this paper will be shared by the lead contact upon request.
- This paper does not report original code.
- Any additional information required to reanalyse the data reported in this paper is available from the lead contact upon request.

METHOD DETAILS

Simulation parameters and conditions

Structurally, an MGDG molecule consists of a polar head, which comprises the β-D-galactose residue and the glycerol backbone, and two α-linolenoyl (di-18:3, *cis*) chains (Figure 1). For galactose, the all-atom optimized potentials for liquid simulations (OPLS-AA) parameters for carbohydrates were used.[66] The acyl chains and glycerol backbone parameters were taken directly from the OPLS-AA force field associated with the GROMACS 5.05 software package,[61] supplemented with partial charges for the polar parts of lipids, that were derived in[67] in the framework of the OPLS-AA force field.

Before MD simulation, each system, described in the section Models, was optimised using the steepest descent algorithm. Energy minimization and simulation were carried out using the package GROMACS 5.05.[61] The electrostatic interactions were evaluated using the particle-mesh Ewald (PME) summation method with a β spline interpolation order of 5 and a direct sum tolerance of 10^{-5}.[68] For calculations of the Ewald sum in real space and the van der Waals (vdW) interactions, a cut-off of 1.0 nm, 3D PBC and the minimum image convention were used.

Simulations were carried out in the isothermal-isobaric NPT ensemble under a constant pressure of 1 bar and at temperatures 295, 333 and 353 K (Tables 1, 2, and S1). In line with our previous practice, the first group of lamellar systems were simulated initially at ambient temperature with anisotropic pressure control. However, due to relatively large systems (the number of atoms was between ∼70 000 and ∼200 000, and ∼900 000) and a relatively short timescale of the simulations (in most cases 1000 ns), to capture transition processes that were the subject of the study, the temperature of the systems was elevated from the initial 295 K to 333 K and to 353 K (80°C), which is the highest temperature at which an experimental study on MGDG polymorphism has been carried out.[5] A CG simulation study of the non-bilayer phases of DOPE indicated that in a multilamellar stack of pure DOPE bilayers at any hydration, increasing the temperature by 20 K in the range between 273 and 320 K increased the rate of stalk formation by a factor of ∼4.[59] In this study, the effect of the increasing temperature was milder.

As a computer model of the lipid bilayer patch is built by replicating lipids in the *x-y* plane, it has axial symmetry relative to the bilayer normal, and as long as it remains lamellar, controlling its pressure semi-isotropically is justified by the geometry. However, due to rotational and translational diffusion of the bilayer lipids, the stress on different simulation box-sides may be different, therefore anisotropic pressure control may be a better choice. In this study, spontaneous transition from the stack of lamellar bilayers to a lattice of water-filled channels is investigated. This transition changes the symmetry of the system and the normal is not an axis of symmetry any more. When starting the simulations, the authors anticipated that pressure anisotropy would give the system more flexibility and facilitate the transition. However, this was not the case. Simulations carried out at room temperature (295 K) and with anisotropic pressure control proceeded without any distortions of

the geometry of the box relative to the initial one. However, when the temperature was increased, in some systems the proportions of the in-plane box dimensions significantly changed (cf. Figures S16 and S17); this prompted us to reconsider the pressure control algorithm used.

Eventually, the first group of systems was initially simulated at 295 K with an anisotropic barostat, then the temperature was increased and the systems that became distorted at higher temperatures were re-simulated (Table 4) and others (Table 2) were simulated with a semiisotropic barostat. The effect of the pressure control algorithm on the behaviour of selected simulation systems and some putative explanation of the behaviour is presented in the section effect of pressure control algorithm.

For the first 1 ns of each simulation, the pressure and temperature were controlled using the Berendsen thermostat and barostat[69] and afterwards using the Nosé-Hoover thermostat[70] and the Parrinello-Rahman barostat[71] with time constants 0.5 ps and 1.0 ps, respectively. The temperatures of the solute and solvent were controlled independently. The linear constraint solver (LINCS) algorithm[72] was used to preserve the length of each covalent bond with a hydrogen atom. This allowed us to use a 2 fs time step when simulation was carried out at 295 K, and 1.5 fs when it was carried out at 333 and 353 K, except for the largest system, 6xW15-15-15, for which the time step was 2 fs. The trajectories were recorded every 1.5 ps when the time step was 1.5 fs, and every 1.0 ps when the time step was 2 fs. The list of nonbonded pairs was updated every 10 steps. The centre-of-mass motion was removed every time step.

To visualize the results the programs PyMOL 1.8.4.[63] and the VMD 1.9.3[62] were used. The scripting language Bash and the domain-specific language AWK[65] were used to process the data and write the scripts for the analyses. The gnuplot software[64] was used to create the graphs. Inkscape[73] was used to assemble, process and modify images obtained from the programs Pymol and VMD.

QUANTIFICATION AND STATISTICAL ANALYSIS

The averages and standard deviations were calculated using AWK. In most cases, numerical data were obtained from 100-ns trajectory fragments, with a 10-ps step unless stated explicitly in the main text. The width of each water layer was estimated as the distance between the cross-points of the lipid and water density distributions (Figure S1A). Each distribution was obtained by dividing the simulation box along the *z*-axis into 1000 slices and in each slice the densities of the lipids or water were calculated using the program GROMACS,[61] generating 1000-point distribution curves. As the height of the simulation box (*z*-axis) was ~12-13 nm (depending on the system), the value of density was determined every 12-13 pm.